

Fast Stabilization of Inducible Magnet Simulation

SEUNG-WOOK KIM, Korea University, South Korea
JUNGHYUN HAN, Korea University, South Korea

This paper presents a novel method for simulating inducible rigid magnets efficiently and stably. In the proposed method, inducible magnets are magnetized by a modified magnetization dynamics, so that the magnetic equilibrium can be obtained in a computationally efficient manner. Furthermore, our model of magnetic forces takes magnetization change into account to produce stable motions of inducible magnets. The experiments show that the proposed method enables a large-scale simulation involving a huge number of inducible magnets.

CCS Concepts: • Computing methodologies → Physical simulation.

Additional Key Words and Phrases: Magnetic fields and forces, rigid body dynamics

ACM Reference Format:

Seung-wook Kim and JungHyun Han. 2022. Fast Stabilization of Inducible Magnet Simulation. *ACM Trans. Graph.* 1, 1 (September 2022), 8 pages. <https://doi.org/10.1145/3550469.3555410>

1 INTRODUCTION

A magnet produces a *magnetic field*, which magnetizes nearby metallic materials. If the magnetized state lasts forever, the materials are called *permanent magnets*. In most materials, however, the magnetization is preserved only when exposed to the magnetic field. These materials, such as iron balls and paperclips, are called *inducible magnets*.

In the computer graphics field, many methods for magnet simulations have been proposed since the seminal work of Thomaszewski et al. [2008]. Among them, the state of the art in simulating *rigid* magnets is the work of Kim et al. [2018]. They introduced the *magnetization dynamics* of inducible magnets, which was widely used in micromagnetics. Their method is able to simulate rigid magnets more effectively and stably than before, but it has limitations. Firstly, due to the non-differentiable nature of their magnetization dynamics and also excessive approximations of the magnetic forces, their simulation may diverge if the magnetic field is excessively strong. Secondly, even though their simulation converges in most cases, the convergence rate may not be fast enough, and a considerable amount of time is often required to reach the equilibrium of magnetization.

In this paper, we propose solutions to the above-mentioned limitations. Our contributions are listed as follows:

Authors' addresses: Seung-wook Kim, Korea University, Seoul, South Korea, wook0249@korea.ac.kr; JungHyun Han, Korea University, Seoul, South Korea, jhan@korea.ac.kr.

Permission to make digital or hard copies of all or part of this work for personal or classroom use is granted without fee provided that copies are not made or distributed for profit or commercial advantage and that copies bear this notice and the full citation on the first page. Copyrights for components of this work owned by others than the author(s) must be honored. Abstracting with credit is permitted. To copy otherwise, or republish, to post on servers or to redistribute to lists, requires prior specific permission and/or a fee. Request permissions from permissions@acm.org.

© 2022 Copyright held by the owner/author(s). Publication rights licensed to ACM. 0730-0301/2022/9-ART \$15.00
<https://doi.org/10.1145/3550469.3555410>

- We model the relation between the magnetic field and magnetization with a differentiable function, which enables the magnetization to change always smoothly as the magnetic field changes.
- We propose a general magnetic-force model, which helps the magnetic simulation converge easily.
- We modify the magnetization dynamics in a way that improves the convergence rates significantly.

2 RELATED WORK

In the computer graphics field, Thomaszewski et al. [2008] presented the first work for magnetic interactions using magnetic moments that are point magnets. Using them, magnetic induction and magnetic forces/torques are calculated. However, their work suffers from instability due to excessively strong magnetic fields. Kim et al. [2018] proposed magnetization dynamics to limit the magnets' strengths, which enable more stable rigid magnet simulations. However, their method just alleviates the instability problem and still suffers from it. On the other hand, Kim and Han [2020] used boundary integral to evaluate magnetic forces and torques for the sake of reducing the time complexity. Their method considers the continuity of magnetization in magnets, enabling more stable rigid magnet simulations. However, it requires numerical integration over polyhedral magnets' boundaries, and the process of integration still consumes a certain amount of time.

Several works have been reported for non-rigid magnet simulations. Ishikawa et al. [2013] simulated magnetic fluids, expressing spikes of the fluid surfaces using energy minimization. Huang et al. [2019] tackled this problem in a different way to produce accurate and effective results. Their method uses unconditionally stable magnetic forces between magnetic particles without diverging forces. Based on the work of Da et al. [2016], Huang and Michels [2020] simulated magnetic fluids using only the liquid surfaces on which magnetic forces are exerted. Ni et al. [2020] proposed a level-set method based on Eulerian simulation to express interactions of magnetic liquids and solids. This method also uses magnetic forces which are exerted on the material's boundaries. Sun et al. [2021] implemented a material point method for nonlinearly magnetized materials using Langevin functions.

3 METHOD

Section 3.1 proposes a general model of the magnetic forces exerted on inducible magnets. The forces are defined in terms of magnetizations, and therefore we need a method to determine them. Section 3.2 summarizes the magnetization dynamics proposed by Kim et al. [2018]. Section 3.3 discusses its limitations and presents our solutions, which enable us to compute the magnetic forces in a robust and efficient manner.

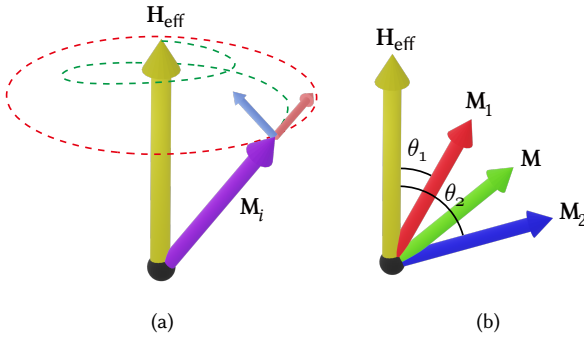


Fig. 1. Magnetization dynamics: (a) Given H_{eff} , each submagnetization, M_i , makes both precessional motion (red arrow) and damping motion (blue arrow). Given the precessional motion only, M_i would keep rotating about H_{eff} (along the dotted red circle). Due to the damping motion, however, M_i 's motion becomes spiral (dotted green). (b) The damping motion of M_i is made through a simple dynamics that updates θ_i . M equals to the average of M_1 and M_2 .

3.1 Magnetic Force

A magnetic object (henceforth, simply magnet) has its own *magnetic moments*. Being vector quantities, they represent the strength of the magnet. Suppose that N magnetic moments are sampled from a magnet, each denoted as \mathbf{m}_i . Given an arbitrary point, p , in the space, let \mathbf{r}_i represent the vector connecting \mathbf{m}_i and p . Then, the *magnetic field*, which we denote as \mathbf{H} , is generated at p by \mathbf{m}_i [Jackson 1999]:

$$\mathbf{H} = \frac{1}{4\pi} \sum_i^N \left(\frac{3\mathbf{r}_i(\mathbf{r}_i \cdot \mathbf{m}_i) - (\mathbf{r}_i \cdot \mathbf{r}_i)\mathbf{m}_i}{\|\mathbf{r}_i\|^5} \right) \quad (1)$$

Consider a magnetic moment, \mathbf{m} , located at p . Its density is called *magnetization*, which we denote as \mathbf{M} , i.e., $\mathbf{M} = \mathbf{m}/V$, where V represents the magnet's volume. Then, the *magnetic flux density*, denoted as \mathbf{B} , is defined as follows:

$$\mathbf{B} = \mu_0 (\mathbf{M} + \mathbf{H}) \quad (2)$$

where μ_0 represents the permeability of the free space. The relation given in Equation (2) is governed by Maxwell's equations.

Magnetic forces are required for rigid-body simulation of magnets. We propose to compute the magnetic forces using *Zeeman energy* [Lakshmanan 2011], which has been widely adopted in the context of micromagnetics. Denoted as E , it is defined as follows:

$$E = -\mathbf{m} \cdot \mathbf{B} \quad (3)$$

Being the negative gradient of E , the magnetic force is expanded as follows:

$$\begin{aligned} \mathbf{F} &= \nabla(\mathbf{m} \cdot \mathbf{B}) \\ &= \mu_0 V \nabla(\mathbf{M} \cdot (\mathbf{M} + \mathbf{H})) \\ &= \mu_0 V \left(\frac{\partial \mathbf{M}}{\partial \mathbf{r}} (2\mathbf{M} + \mathbf{H}) + \frac{\partial \mathbf{H}}{\partial \mathbf{r}} \mathbf{M} \right) \\ &= \mu_0 V \left(\frac{\partial \mathbf{M}}{\partial \mathbf{H}} \frac{\partial \mathbf{H}}{\partial \mathbf{r}} (2\mathbf{M} + \mathbf{H}) + \frac{\partial \mathbf{H}}{\partial \mathbf{r}} \mathbf{M} \right) \end{aligned} \quad (4)$$

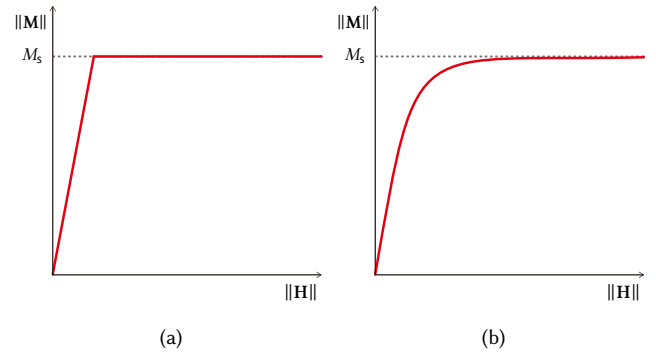


Fig. 2. Magnetization curves: (a) Non-differentiable curve in Kim et al. [2018]. (b) Our differentiable curve.

As $\frac{\partial \mathbf{H}}{\partial \mathbf{r}}$ can be analytically obtained from Equation (1), $\frac{\partial \mathbf{M}}{\partial \mathbf{H}}$ remains as the only unknown term in Equation (4). In Section 3.3, we will define the magnetization, \mathbf{M} , as a function of \mathbf{H} so that $\frac{\partial \mathbf{M}}{\partial \mathbf{H}}$ can be computed.

3.2 Magnetization Dynamics

This subsection briefly presents the magnetization dynamics implemented by Kim et al. [2018]. For magnetic induction, they used the so-called *effective magnetic field*, denoted as H_{eff} . It is comprised of both external and internal (self-exerting) magnetic fields, and its simple form is expressed as follows:

$$H_{\text{eff}} = \mathbf{H} - \gamma_D \mathbf{M} \quad (5)$$

where γ_D is the self-demagnetizing factor. For a spherically shaped magnetic moment, $\gamma_D = 1/3$.

The magnetization, \mathbf{M} , of a single magnetic moment is decomposed into two submagnetizations, M_1 and M_2 . Given H_{eff} evaluated at the magnetic moment, Landau-Lifshitz-Gilbert (LLG) equation [Gilbert 1955] is used to simulate M_i 's dynamics:

$$\frac{d\mathbf{M}_i}{dt} = -\frac{\gamma}{1+\alpha^2} \left(\mathbf{M}_i \times \mathbf{H}_{\text{eff}} + \alpha \mathbf{M}_i \times (\mathbf{M}_i \times \mathbf{H}_{\text{eff}}) \right) \quad (6)$$

where γ is the gyromagnetic ratio, and α is the material-specific damping constant that is between 0.2 and 0.25 in the current implementation. Once M_1 and M_2 are updated, their average is taken as M .

In Equation (6), $\mathbf{M}_i \times \mathbf{H}_{\text{eff}}$ represents the *precessional motion* whereas $\mathbf{M}_i \times (\mathbf{M}_i \times \mathbf{H}_{\text{eff}})$ does the *damping motion*. See Fig. 1-(a). Using the damping motion, the dynamics tries to align M_i with H_{eff} .

Through Equations (5) and (6), M converges, and the relation between \mathbf{M} and \mathbf{H} is defined as follows:

$$\mathbf{M} = \begin{cases} \frac{1}{\gamma_D} \mathbf{H} & \text{if } \|\mathbf{H}\| < \gamma_D M_s \\ \frac{M_s}{\|\mathbf{H}\|} \mathbf{H} & \text{otherwise} \end{cases} \quad (7)$$

where M_s represents the maximum magnitude of magnetization. Fig. 2-(a) depicts the magnetization curve defined by Equation (7).

3.3 Problems of Magnetization Dynamics and Our Solutions

The magnetization dynamics presented in Section 3.2 reveals several problems. Firstly, its convergence rate is not fast enough. It is mainly due to the precessional motion depicted in Fig. 1-(a). Our solution is to discard the precessional motion and take only the damping motion. If we used the damping term in Equation (6) as is, however, we would still suffer from numerical errors because the damping motions are not circular. The stronger \mathbf{H}_{eff} is, the larger the errors are. Worse still, the errors may also affect nearby inducible magnets, often resulting in chaotic \mathbf{H}_{eff} , which eventually prevents the magnetization dynamics from being converged.

We tackle this problem by adopting a simple dynamics that guarantees “circular damping motions” of \mathbf{M}_i . Let us denote the angle between \mathbf{H}_{eff} and \mathbf{M}_i as θ_i , as shown in Fig. 1-(b), and define the time derivative of θ_i as follows:

$$\frac{d\theta_i}{dt} = -\beta \|\mathbf{H}_{\text{eff}}\| \Theta(\theta_i) \quad (8)$$

where β is a user-defined damping coefficient that is set to 0.005 in our implementation, and

$$\Theta(\theta_i) = \begin{cases} \sin \theta_i & \text{if } |\theta_i| < \pi/2 \\ 2 - \sin \theta_i & \text{otherwise} \end{cases} \quad (9)$$

The trigonometric functions are derived from the double cross product of \mathbf{M}_i with \mathbf{H}_{eff} in Equation (6). The updated θ_i updates \mathbf{M}_i , and the average of \mathbf{M}_1 and \mathbf{M}_2 is taken as \mathbf{M} .

Ignoring the precessional motion would make our magnetization dynamics physically less correct. However, the experiment results reported in Section 5 are visually pleasing and show no noticeable artifacts, compared with the simulation results of the previous works.

Another problem of the magnetization dynamics proposed by Kim et al. [2018] is that the magnetization curve depicted in Fig. 2-(a) is not smooth. In principle, the magnetization curve should be smooth, i.e., differentiable, as shown in Fig. 2-(b). Otherwise, magnetic fields, magnetizations and resulting magnetic forces become non-differentiable, which may often prevent the magnets’ motions from being smooth.

In our method, the smooth magnetization curve depicted in Fig. 2-(b) is modeled with a hyperbolic tangent function:

$$\begin{aligned} \mathbf{M} &= f(\mathbf{H}) \\ &= \frac{M_s}{\|\mathbf{H}\|} \tanh\left(\frac{3}{M_s} \|\mathbf{H}\|\right) \mathbf{H} \end{aligned} \quad (10)$$

\mathbf{M} is differentiable, enabling us to evaluate $\frac{\partial \mathbf{M}}{\partial \mathbf{H}}$ in Equation (4) at any time.

Equation (10) is devised so that the differential curve resembles the non-differential one in Fig. 2-(a) as much as possible. They share not only the saturated magnetization’s magnitude, M_s , but also the initial slope. Equation (10) asserts that the initial slope of the differentiable curve is three. On the other hand, Equation (7) asserts that the slope of the non-differentiable curve shown in Fig. 2-(a) remains as $\frac{1}{\gamma_D}$ before saturation. For a spherical magnetic moment, $\gamma_D = 1/3$, making the slope also three.

```

repeat
  for each magnetization M = {M1, M2} do
    compute H using Equation (1)
    compute Heff using Equation (11)
    integrate theta_i using Equation (8)
    update Mi from theta_i
  end
until every M converges;
for each pair of magnetic moments do
  | compute F using Equation (4)
end

```

Algorithm 1: Magnetic simulation.

As we replace Equation (7), which contains γ_D , by Equation (10), we need to redefine \mathbf{H}_{eff} (given in Equation (5)) without using γ_D . Noting again that γ_D represents the inverse slope of the magnetization curve, \mathbf{H}_{eff} is redefined as follows:

$$\mathbf{H}_{\text{eff}} = \mathbf{H} - \gamma_C \mathbf{M} \quad (11)$$

where $\gamma_C = \|f^{-1}(\mathbf{M})\|$.

Unfortunately, γ_C in Equation (11) may become excessively large if the derivative of $\|f(\mathbf{H})\|$ becomes close to zero. We resolve this problem by defining the upper bound of γ_C ; If the derivative of $\|f(\mathbf{H})\|$ is nearly zero, i.e., if $\|\mathbf{M}\|$ almost reaches the maximum magnitude of magnetization, M_s , γ_C is clamped to the upper bound.

4 IMPLEMENTATION

Algorithm 1 shows the magnetic simulation steps. Each magnet is sampled with magnetic moments. On the position of each magnetic moment, the magnetic field, \mathbf{H} , is computed using Equation (1). Given the magnetization, \mathbf{M} , of the magnetic moment, the effective magnetic field, \mathbf{H}_{eff} , is calculated using Equation (11). Given \mathbf{H}_{eff} , θ_i is updated using Equation (8), and then \mathbf{M}_i is defined by θ_i . After all magnetizations converge, the magnetic forces are computed using Equation (4) and then are sent to the rigid-body solver.

Equation (10) asserts that \mathbf{M} of an inducible magnet is aligned with \mathbf{H} . Because magnetic torque occurs only when \mathbf{M} is not aligned with \mathbf{H} , magnetic torque of an inducible magnet is not handled at all in **Algorithm 1**.

5 EXPERIMENT RESULTS

Our experiments are all made with Intel Core i7-8700 3.20 GHz CPU and 32 GB memory. Bullet Physics [Coulmans 2015] is used for rigid-body simulation with the time step size of 1ms whereas magnetic simulation is made with that of 30~200ns. All scenes are rendered using Mitsuba [Jakob 2010]. The accompanying video shows all experiments presented in this section.

The method of Kim et al. [2018] produces good results when the magnetic forces are moderately strong. If they are made excessively strong (e.g., for generating an impressive scene), however, it may become unstable. All experiments reported in this section are made with excessively strong magnets, and the simulation results of our method are compared with those of Kim et al. [2018]. Section 6.1 will rigorously discuss why our method outperforms [Kim et al. 2018].

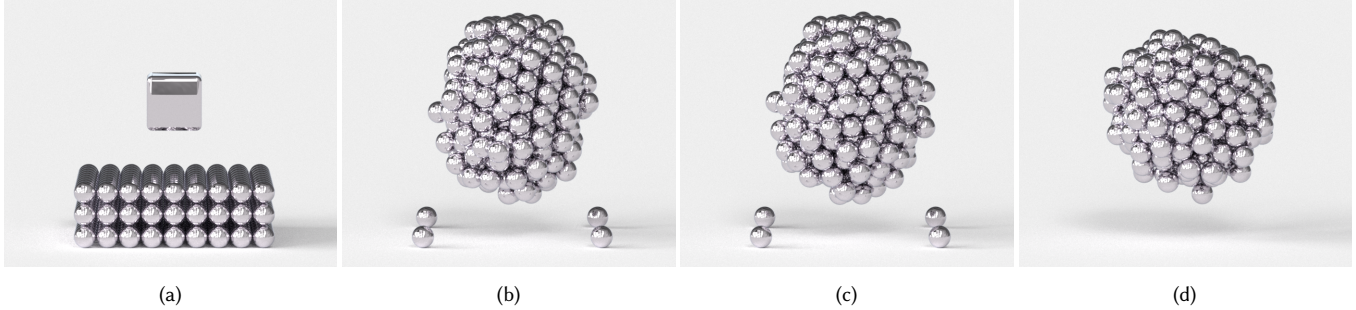


Fig. 3. **[Balls Up]** A mid-air cube magnet attracts a number of iron balls: (a) Initial state. (b)-(c) The results of [Kim et al. 2018]. (d) Ours.

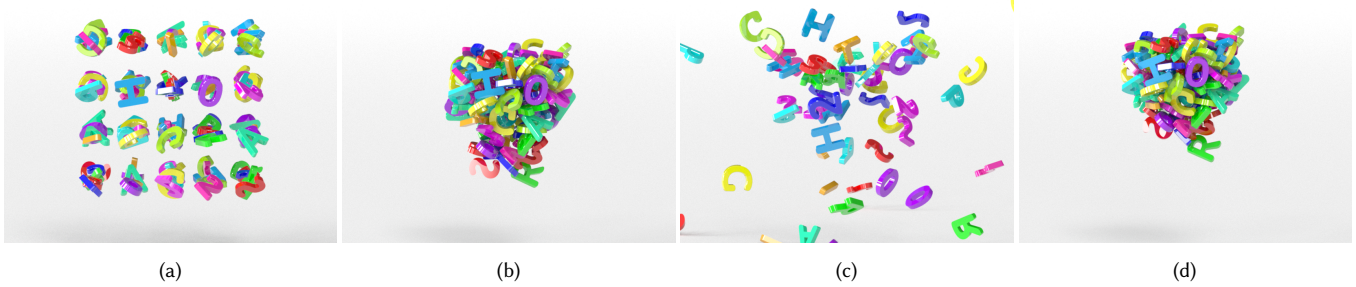


Fig. 4. **[Alphabets]** An invisible excessively-strong magnetic moment is located at the center of the alphabet magnets: (a) Initial state. (b) In both [Kim et al. 2018] and our method, the alphabets initially get together. (c) In [Kim et al. 2018], however, the alphabets are blown up immediately. (d) In contrast, our method runs the simulation stably.

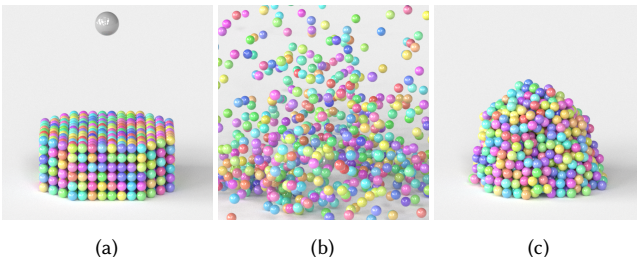


Fig. 5. **[Falling Magnet]** A heavy and strong sphere magnet falls down and strikes the metal balls: (a) Initial state. (b) The result of [Kim et al. 2018]. (c) Ours.

In both our method and [Kim et al. 2018], the magnetic forces diverge if $\|r_i\|$ in Equation (1) becomes close to zero. In such a case, a small fraction, ϵ^2 , is added to $\|r_i\|^5$ in the denominator. It is informally called a smoothing operation.

Balls Up. Fig. 3-(a) shows the initial state of a mid-air neodymium magnet and a stack of 243 ($9 \times 9 \times 3$) iron balls on the ground. Being a permanent magnet, the neodymium magnet is quite strong in general. It will magnetize and pull up the balls. No friction is used in this experiment because our purpose is to assess the stability of magnetic simulation without the aid of friction. Fig. 3-(b) and (c) show the results of [Kim et al. 2018]. The iron balls are successfully attracted by the neodymium magnet but they do not settle down.

The balls keep vibrating and even rotate around the neodymium magnet. In contrast, Fig. 3-(d) shows the result of our method, where the iron balls are stably stuck to each other and to the neodymium magnet.

Alphabets. Fig. 4-(a) shows a group of mid-air alphabet-shaped inducible magnets. We have 100 alphabets structured in a 3D grid of $5 \times 5 \times 4$ points. Once an invisible but excessively strong magnetic moment is located at the center of the grid, it magnetizes the alphabets so that they get together, as shown in Fig. 4-(b). In [Kim et al. 2018], however, the alphabets are then rapidly separated from each other and blown up, as shown in Fig. 4-(c). In contrast, the simulation remains stable in our method, as shown in Fig. 4-(d).

Falling Magnet. In Fig. 5-(a), a heavy and strong magnet is above a stack of 1032 metal balls on the ground. It falls and strikes the balls. Fig. 5-(b) shows the result of [Kim et al. 2018], where the balls are scattered due to unstable simulation. In contrast, Fig. 5-(c) shows the result of our stable simulation method.

Sakura Tree. In Fig. 6, 2500 iron balls are falling from the sky and are attracted by the tree magnet. A magnetic moment is attached to the end of each branch so that the falling balls are stuck around the branch ends. This experiment demonstrates our method's capability of running a large-scale simulation stably.

For the experiments presented so far, Table 1 reports the average times measured in milliseconds “per frame” which are spent for

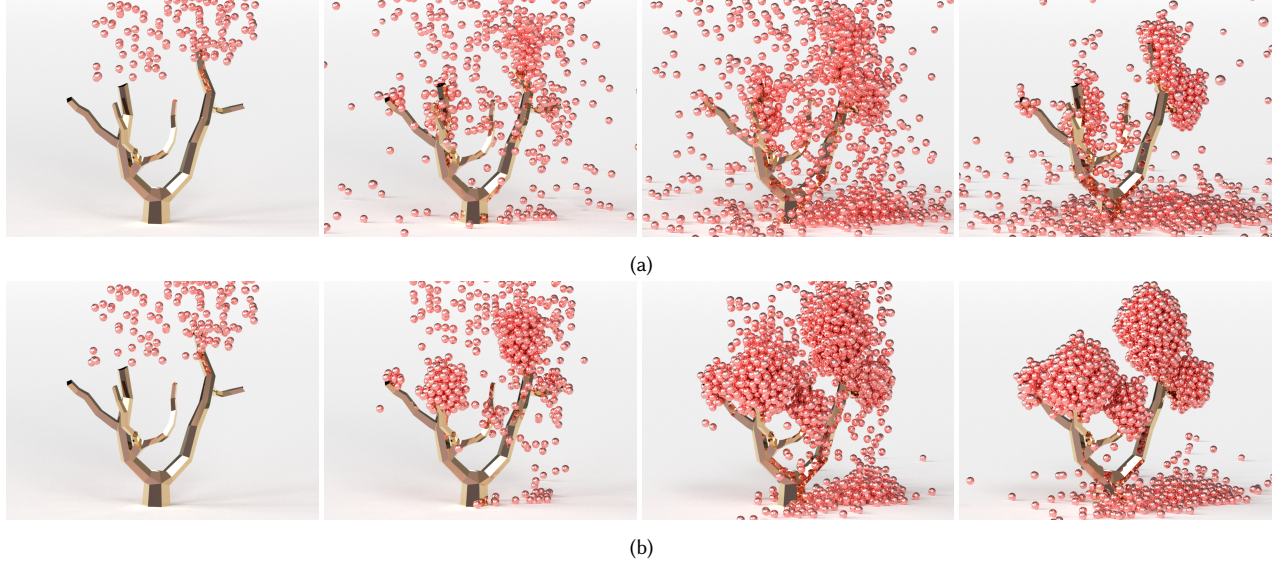


Fig. 6. [Sakura Tree] A number of iron balls fall down and stick to the tree magnet: (a) The results of [Kim et al. 2018]. (b) Our method enables a large-scale simulation to run stably.

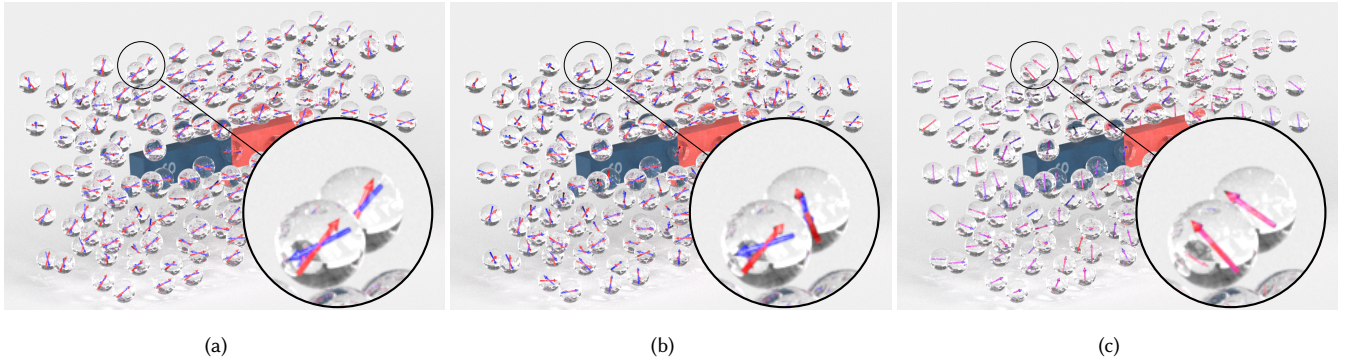


Fig. 7. Convergence of M_1 and M_2 : (a) Initial state. (b) The result of [Kim et al. 2018]. (c) Ours.

Table 1. Performance measurements: T_i , T_f and T_r represent the times (in milliseconds) spent for magnetic induction, magnetic-force computation and rigid-body simulation, respectively.

Scene	[Kim et al. 2018]			Our method		
	T_i	T_f	T_r	T_i	T_f	T_r
<i>Balls Up</i> (Fig. 3)	20	3.5	14	1.8	3.8	14
<i>Alphabets</i> (Fig. 4)	3.3	1.3	15	1.3	1.4	110
<i>Falling Magnet</i> (Fig. 5)	251	58	59	36	61	60
<i>Sakura Tree</i> (Fig. 6)	778	97	65	61	101	75

magnetic induction (T_i), magnetic-force computation (T_f) and rigid-body simulation (T_r). For example, T_i of [Kim et al. 2018] in *Balls Up* is measured for 1000 frames, and their average is 20 milliseconds. In all experiments, T_i in our method are significantly smaller than those of [Kim et al. 2018] because our magnetization dynamics does

not consider the precessional motions of submagnetizations. Table 1 shows that in *Alphabets*, T_r of ours is much larger than that of [Kim et al. 2018]. It is devoted to resolving collisions between alphabets. In [Kim et al. 2018], the alphabets are blown up, as shown in Fig. 4-(c), and therefore the rigid-body simulator remains largely idle.

Fig. 7-(a) shows a set of crystal balls around a strong bar magnet. In each ball, the submagnetizations, M_1 and M_2 , are visualized in red and blue vectors. Whereas the balls are fixed in the space, the submagnetizations are updated, i.e., rotated, not only by the magnetic field generated by the bar magnet but also by the magnetic fields generated by the other balls' magnetizations. Fig. 7-(b) shows the oscillating and divergent submagnetizations simulated by [Kim et al. 2018], and Fig. 7-(c) shows the result of our method, where the dynamics quickly converges. Because our magnetization dynamics does not include precessional motions and alleviates numerical errors, it enables fast convergence of magnetization.

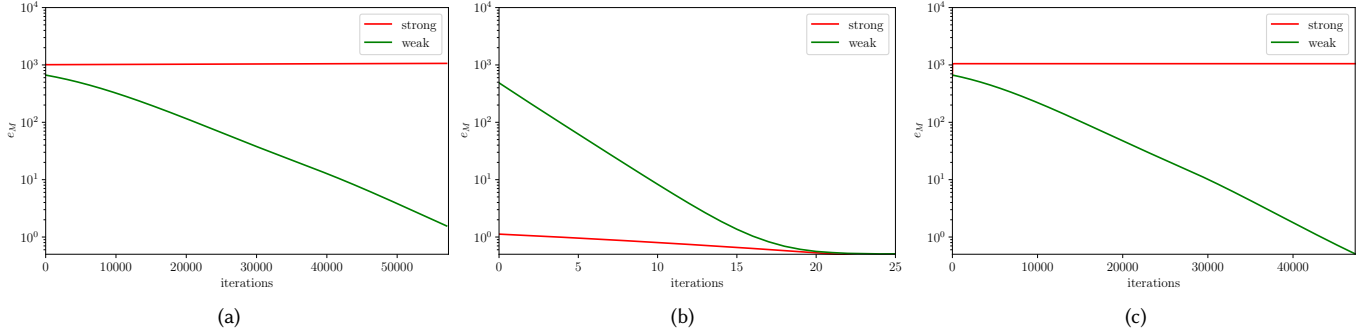


Fig. 8. In the experiment setup of Fig. 7 with two distinct strengths of the bar magnet, the magnetization errors, e_M , are measured through iterations: (a) Errors in [Kim et al. 2018]. (b) Ours. (c) Errors in damping-only LLG.

Given \mathbf{M} updated by magnetization dynamics, the *magnetization error*, which we denote as e_M , is defined as follows:

$$e_M = \frac{\|\mathbf{M}_{gt} - \mathbf{M}\|}{\|\mathbf{M}_{gt}\|} \quad (12)$$

where \mathbf{M}_{gt} is the groundtruth magnetization. In [Kim et al. 2018], \mathbf{M}_{gt} is computed using Equation (7). In our method, it is computed using Equation (10).

In the experimental setup shown in Fig. 7, e_M is evaluated. Fig. 8-(a) shows two curves of e_M in [Kim et al. 2018]; the red curve depicts e_M measured with a strong bar magnet, i.e., with a strong magnetic field, and the green one is with a weak bar magnet. The red curve shows that the strong magnet field prevents the magnetization dynamics of [Kim et al. 2018] from being converged. On the other hand, given a weak magnetic field, e_M decreases through iterations, but the decreasing rate is slow, i.e., the magnetization dynamics converges slowly. In contrast, Fig. 8-(b) shows that our magnetization dynamics converges fast regardless of the magnetic field strengths.

As discussed in Section 3.3, taking only the damping motion in Equation (6) as is, which we call *damping-only LLG*, would also suffer from numerical errors. Fig. 8-(c) shows the test results. As in [Kim et al. 2018], the damping-only LLG does not converge under the strong magnetic field. Given a weak magnetic field, it converges a little faster than [Kim et al. 2018] because it is free from the numerical errors brought by the precessional motion.

In the same experimental setup shown in Fig. 7, let us see how our method, [Kim et al. 2018] and damping-only LLG work with varying parameters. In Fig. 7, the time step size, Δt , is set to 100ns. Now, it is multiplied by 1.0 up to 1.5 in steps of 0.01. The horizontal axis in Fig. 9 represents such 51 distinct time steps. On the other hand, the vertical axis in Fig. 9 is for the magnetic field's strength, $\|\mathbf{H}\|$. In this test, it is made to be a multiple of $\|\mathbf{M}\|$. The multiplier ranges from 0.0 to 10.0 in steps of 0.01, i.e., we have 1001 distinct values of $\|\mathbf{H}\|$. In total, we have 51×1001 combinations of Δt and $\|\mathbf{H}\|$. For a combination, 10,000 tests are made, each with a randomly selected direction of \mathbf{H} , and the average of the iteration counts is depicted in rainbow colors, VIBGYOR, where Violet implies a single iteration and Red implies more than 999 iterations or a failure case. Fig. 9 shows that our method is superior to [Kim et al. 2018] and the damping-only LLG.

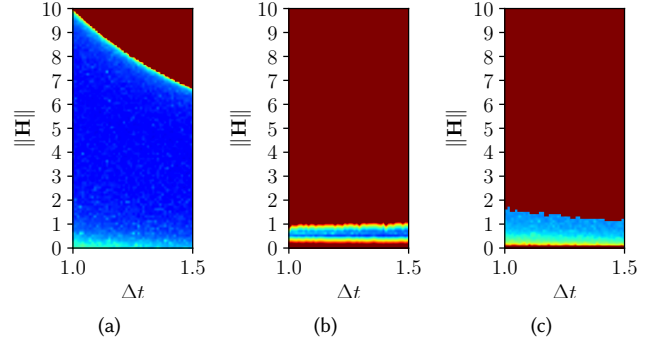


Fig. 9. The iteration counts are color-coded in the 2D space spanned by Δt and $\|\mathbf{H}\|$. (a) Our method. (b) [Kim et al. 2018]. (c) Damping-only LLG.

6 DISCUSSION

6.1 Magnetic Force and Magnetization Dynamics

This subsection shows that the force model adopted in most of the previous works [Huang et al. 2019; Kim and Han 2020; Kim et al. 2018; Sun et al. 2021; Thomaszewski et al. 2008] is excessively approximated and the simulation in the method of Kim et al. [2018] may not converge easily. Our method does not suffer from the problems; this explains why our method outperforms the method of Kim et al. [2018] in the experiments presented in Section 5.

In most of the previous works, the magnetic force, \mathbf{F} , is defined as follows:

$$\mathbf{F} = \mu_0 \mathbf{m} \cdot \nabla \mathbf{H} \quad (13)$$

Plugging \mathbf{H} given in Equation (1) into Equation (13) returns the following:

$$\begin{aligned} \mathbf{F} = & \frac{\mu_0}{4\pi} \sum_i^N \left[\frac{-15\mathbf{r}_i((\mathbf{m} \cdot \mathbf{r}_i) \cdot (\mathbf{m}_i \cdot \mathbf{r}_i))}{\|\mathbf{r}_i\|^7} \right. \\ & \left. + \frac{3\mathbf{r}_i(\mathbf{m} \cdot \mathbf{m}_i) + 3(\mathbf{m}(\mathbf{m}_i \cdot \mathbf{r}_i) + \mathbf{m}_i(\mathbf{m} \cdot \mathbf{r}_i))}{\|\mathbf{r}_i\|^4} \right] \end{aligned} \quad (14)$$

It is the force exerted on \mathbf{m} by \mathbf{m}_i . This force model assumes that both \mathbf{m}_i and \mathbf{m} are *constants*. However, \mathbf{m}_i may change via magnetization

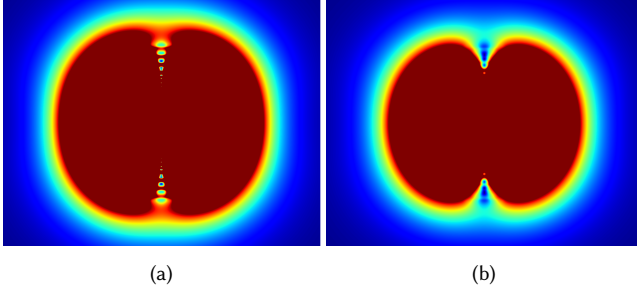


Fig. 10. Visualization of magnetic force field over a cross section of a spherical magnet, which is uniformly magnetized. The magnitudes of the force field are in rainbow colors, **VIBGYOR**, where **Violet** is the weakest and **Red** is the strongest. (a) The result of [Kim et al. 2018]. (b) Ours.

dynamics and even their positions may change, i.e., \mathbf{r}_i may change. The same applies also to \mathbf{m} . \mathbf{F} given in Equation (14) would work if all of \mathbf{m} , \mathbf{m}_i and \mathbf{r}_i were fixed. In general, however, magnets continuously move, resulting in dynamically changing \mathbf{m} , \mathbf{m}_i and \mathbf{r}_i . \mathbf{F} in Equation (14) is excessively approximated, making it not easy for rigid-body dynamics as well as magnetization dynamics to converge.

In our method, $\mathbf{F} = \nabla(\mathbf{m} \cdot \mathbf{B})$ as defined in Equation (4), i.e., magnetic moments and equivalently magnetizations are taken as *variables*. In Equation (4), the spatial derivative, $\frac{\partial \mathbf{M}}{\partial \mathbf{r}}$, implies that our method allows \mathbf{M} to change its position; In more detail, $\frac{\partial \mathbf{M}}{\partial \mathbf{r}}$ is rephrased as $\frac{\partial \mathbf{M}}{\partial \mathbf{H}} \frac{\partial \mathbf{H}}{\partial \mathbf{r}}$ so that \mathbf{r} 's change causes \mathbf{H} 's change which then causes \mathbf{M} 's change. In addition to this rigid-body dynamics, note that our magnetization dynamics makes \mathbf{H} independently change \mathbf{M} .

Recall that \mathbf{M}_i is aligned with \mathbf{H}_{eff} via magnetization dynamics. Then, \mathbf{M}_1 tends to equal \mathbf{M}_2 , maximizing \mathbf{M} that is defined as the average of \mathbf{M}_1 and \mathbf{M}_2 . On the other hand, our \mathbf{F} is along $\nabla(\mathbf{M}^2)$, as can be found in Equation (4), i.e., \mathbf{F} also tries to maximize the strength of \mathbf{M} . The magnetization dynamics and the magnetic force work together for maximizing \mathbf{M} , making our simulation stabilized quickly.

In Equation (13), \mathbf{F} is defined in terms of \mathbf{H} . In contrast, our method defines \mathbf{F} in terms of \mathbf{B} (in Equation (4)), which is defined in terms of \mathbf{M} as well as \mathbf{H} (in Equation (2)). Then, it might be argued that the ‘additional’ \mathbf{M} may cause excessively strong magnetic forces. In reality, the opposite is true. Fig. 2-(b) shows that $\frac{\partial \mathbf{M}}{\partial \mathbf{H}}$ decreases as the magnitude of \mathbf{M} increases. Such decreasing $\frac{\partial \mathbf{M}}{\partial \mathbf{H}}$ reduces \mathbf{F} in Equation (4). Fig. 10 visualizes magnetic forces over a cross section of a spherical magnet. Not surprisingly, the forces generated by the method of Kim et al. [2018] (shown in Fig. 10-(a)) are stronger than those generated by our method (shown in Fig. 10-(b)).

Finally, note that the force, \mathbf{F} , defined as $\mu_0 \mathbf{m} \cdot \nabla \mathbf{H}$ in Equation (13) is a simplified form of our \mathbf{F} , defined as $\nabla(\mathbf{m} \cdot \mathbf{B})$ in Equation (4). Because $\mathbf{B} = \mu_0 (\mathbf{M} + \mathbf{H})$ (in Equation (2)), $\mathbf{F} = \nabla(\mathbf{m} \cdot \mathbf{B}) = \mu_0 \nabla(\mathbf{m} \cdot (\mathbf{M} + \mathbf{H}))$. When \mathbf{m} and \mathbf{M} are assumed to be constant, as done in most of the previous works, $\mathbf{F} = \mu_0 \mathbf{m} \cdot \nabla \mathbf{H}$. Our force model is a generalization of the force model used in the previous works.

6.2 Magnetization Curve

An alternative to Equation (10) might be the Langevin function used in the work of Sun et al. [2021]. Denoted as $\mathcal{L}(x)$, it is defined as $\coth x - x^{-1}$. In our study, the first trial was to define the differentiable magnetization curve using $\mathcal{L}(x)$. However, we found that $\mathcal{L}(x)$ is computationally unstable, i.e., the function is error-prone when x is nearly zero. The same problem is encountered if we compute the derivative of $\mathcal{L}(x)$.

6.3 Uniqueness of Magnetization Dynamics Solutions

Our magnetization dynamics is modeled with an intuitive approach, and discarding the precessional motion may be taken as physically less correct. Unfortunately, there is no analytic solution of magnetization dynamics due to its complexity, and therefore we cannot verify our numerical solution by comparing it with the analytic one.

In the recent works [Huang et al. 2019; Huang and Michels 2020; Ni et al. 2020; Sun et al. 2021], it has been experimentally proved that there is a unique solution per environment with respect to magnetostatics. Recall that given the weak bar magnet in Fig. 8, both the method of Kim et al. [2018] and our method converged. For each of 178 crystal balls, we computed $\|\mathbf{M}_K - \mathbf{M}_O\| / \|\mathbf{M}_K\|$, where \mathbf{M}_K denotes the magnetization of the method of Kim et al. [2018] and \mathbf{M}_O denotes that of our method. Its average is around 0.0008, i.e., 0.08%, which represents a negligible error. Even though this validates practically the uniqueness of magnetization dynamics solutions, we acknowledge that the physical motivation for our method has not been completely verified. A full understanding of why our method works is a future research topic.

7 CONCLUSION

We proposed a method for simulating inducible rigid magnets in an efficient and stable way. In the method, each magnet becomes induced by a novel magnetization dynamics, which does not take the precessional motions into account but considers only the damping motions, so that the dynamics easily converges. Furthermore, our magnetic-force model is devised to be sensitive to magnetization change so that the distribution of magnetizations can quickly reach its equilibrium. These features enable more stable motions of magnets in an efficient way.

However, our method has several limitations in addition to the fundamental issue discussed in Section 6.3. Our method focuses on inducible magnets, not on permanent magnets. Given a scene mainly composed of permanent magnets, for example, our method may not excel the previous works. In addition, even though our method seldom diverges, it is not completely free from accumulation of numerical error, due to the time-stepping scheme of rigid-body simulation. Our future work will be made to resolve these issues.

ACKNOWLEDGMENTS

This research was supported by Samsung Research Funding & Incubation Center of Samsung Electronics under Project Number SRFC-IT1902-07 and also by the Ministry of Science and ICT, Korea, under the ICT Creative Consilience Program (IITP-2022-2020-0-01819), ITRC (Information Technology Research Center) Support Program (IITP-2022-2020-0-01460) and the grant No.2020-0-00861.

REFERENCES

- E Coumans. 2015. Bullet physics simulation. In *ACM SIGGRAPH 2015 Courses*. ACM, 7.
- F Da, D Hahn, C Batty, C Wojtan, and E Grinspun. 2016. Surface-only liquids. *ACM Transactions on Graphics (TOG)* 35, 4 (2016), 1–12.
- TL Gilbert. 1955. A Lagrangian formulation of the gyromagnetic equation of the magnetization field. *Phys. Rev.* 100 (1955), 1243.
- L Huang, T Hädrich, and DL Michels. 2019. On the Accurate Large-scale Simulation of Ferrofluids. *ACM Transactions on Graphics (TOG)* 38, 4 (2019), 93.
- L Huang and DL Michels. 2020. Surface-only ferrofluids. *ACM Transactions on Graphics (TOG)* 39, 6 (2020), 1–17.
- T Ishikawa, Y Yue, K Iwasaki, Y Dobashi, and T Nishita. 2013. Visual Simulation of Magnetic Fluid Using a Procedural Approach for Spikes Shape. In *Computer Vision, Imaging and Computer Graphics. Theory and Application*. Springer, 112–126.
- JD Jackson. 1999. Classical electrodynamics. *American Journal of Physics* 67, 9 (1999), 841–842.
- W Jakob. 2010. Mitsuba renderer. <http://www.mitsuba-renderer.org>.
- S Kim and J Han. 2020. Simulation of Arbitrarily-shaped Magnetic Objects. In *Computer Graphics Forum*, Vol. 39. Wiley Online Library, 119–130.
- S Kim, S Park, and J Han. 2018. Magnetization dynamics for magnetic object interactions. *ACM Transactions on Graphics (TOG)* 37, 4 (2018), 121.
- M Lakshmanan. 2011. The fascinating world of the Landau–Lifshitz–Gilbert equation: an overview. *Philosophical Transactions of the Royal Society A: Mathematical, Physical and Engineering Sciences* 369, 1939 (2011), 1280–1300.
- X Ni, B Zhu, B Wang, and B Chen. 2020. A Level-Set Method for Magnetic Substance Simulation. *ACM Transactions on Graphics (TOG)* 39, 4 (2020).
- Y Sun, X Ni, B Zhu, B Wang, and B Chen. 2021. A material point method for nonlinearly magnetized materials. *ACM Transactions on Graphics (TOG)* 40, 6 (2021), 1–13.
- B Thomaszewski, A Gumann, S Pabst, and W Strasser. 2008. Magnets in Motion. In *ACM SIGGRAPH Asia 2008 Papers* (Singapore) (*SIGGRAPH Asia '08*). ACM, New York, NY, USA, Article 162, 9 pages. <https://doi.org/10.1145/1457515.1409115>